Estimating geostatistical parameters and spatially-variable hydraulic conductivity within a catchment system using an ensemble smoother

R. T. Bailey and D. Baù

Department of Civil and Environmental Engineering, Colorado State University, USA

Correspondence to: R. T. Bailey (rtbailey@engr.colostate.edu)

Abstract. Groundwater flow models are important tools in assessing baseline conditions and investigating management alternatives in groundwater systems. The usefulness of these models, however, is often hindered by insufficient knowledge regarding the magnitude and spatial distribution of the spatially-distributed parameters, such as hydraulic conductivity (K), that govern the response of these models. Proposed parameter estimation methods frequently are demonstrated using simplified aquifer representations, when in reality the groundwater regime in a given watershed is influenced by strongly-coupled surface-subsurface processes. Furthermore, parameter estimation methodologies that rely on a geostatistical structure of K often assume the parameter values of the geostatistical model as known or estimate these values from limited data.

In this study, we investigate the use of a data assimilation algorithm, the Ensemble Smoother, to provide enhanced estimates of K within a catchment system using the fully-coupled, surface-subsurface flow model CATHY. Both water table elevation and streamflow data are assimilated to condition the spatial distribution of K. An iterative procedure using the ES update routine, in which geostatistical parameter values defining the true spatial structure of K are identified, is also presented. In this procedure, parameter values are inferred from the updated ensemble of K fields and used in the subsequent iteration to generate the K ensemble, with the process proceeding until parameter values are converged upon. The parameter estimation scheme is demonstrated via a synthetic three-dimensional tilted v-shaped catchment system incorporating stream flow and variably-saturated subsurface flow, with spatio-temporal variability in forcing terms. Results indicate that the method is successful in providing improved estimates of the K field, and that the iterative scheme can be used to identify the geostatistical parameter values of the aquifer system. In general, water table data have a much greater ability than streamflow data to condition K. Future research includes applying the methodology to an actual regional study site.

1 Introduction

1.1 Inverse modeling in groundwater applications

Hydrologic models are important tools in assessing baseline conditions and investigating best-management practices in groundwater and catchment-scale systems. Before reliable hydrologic assessments can be made, however, parameter values that drive the response of the model must be appropriately chosen for a specific aquifer or catchment. Direct measurements of hydrologic parameters, however, are scarce and fraught with uncertainty, and typically only apply locally due to the spatial variability of parameter values.

To address this problem of parameter uncertainty, hydrologic models can be used in applications "opposite" or "inverse" to their original use, i.e., parameter values are treated as system unknowns and are determined by extracting

information from observations of system-response variables (Kitanidis and Vomvoris, 1983). The general approach consists of determining the set of parameter values that yields adequate matches between model results and observations from the true hydrologic system. The treatment of parameter values as unknowns that need to be identified constitutes the inverse problem of groundwater modeling (Kitanidis and Vomvoris, 1983), and in most cases must be incorporated in the modeling process (Carrera et al., 2005).

In recent decades numerous methodologies have been proposed and applied to the inverse modeling problem in groundwater modeling, with the general aim to estimate the spatial distribution of hydraulic conductivity (K) or transmissivity (T) in an aquifer system. An excellent review of early inverse methods is provided by Carrera and Neuman (1986). A review of more recently-proposed methods is given by Carrera et al. (2005). Broadly, parameter estimation is accomplished either through (i) optimization procedures, in which an objective function is defined (typically minimizing the error between model results and measurements) and minimized in a least-squares approach, and (ii) statistical conditioning, in which covariance between the parameters and system-response variables is utilized to condition the parameter values using measurement information. It should be noted that conditioning methods also incorporate a sense of optimization, although the optimization occurs in the derivation of the conditioning algorithm, e.g., through minimizing the trace of the a posteriori error estimate covariance matrix (e.g., Kalman, 1960).

For the optimization classification, methods include zonation, the pilot point method (e.g., RamaRao et al., 1995), the represent method (RM) (Bennett, 1992; Valstar et al., 2004), and the self-calibrated method (SCM) (Hendricks Franssen et al., 1999; Gómez-Hernández et al., 2003). For the statistical conditioning classification, methods include Cokriging (e.g., Ahmed and De Marsily, 1993; Li and Yeh, 1999) and data assimilation techniques, such as the family of Kalman Filter (Kalman, 1960) methods, including the Extended Kalman Filter (EKF) (Evensen, 1992), the Ensemble Kalman Filter (EnKF) (Evensen, 1994, 2003), the Ensemble Kalman Smoother (EnKS) (Evensen and van Leeuwen, 2000), and the Ensemble Smoother (ES) (van Leeuwen and Evensen, 1996). The EnKF has particularly been used in recent years to estimate state parameters. Comparisons between the RM and EnKF methods are given by Reichle et al. (2002) and Ngodock et al. (2006). A comparison between the SCM and EnKF methods is provided by Hendricks Franssen and Kinzelbach (2009).

Proposed methodologies are demonstrated typically using simplified hydrologic systems. For applications to groundwater systems, the majority of methodologies are demonstrated using two-dimensional (2-D) confined groundwater flow models (e.g., Gailey et al., 1991; Hantush and Mariño, 1997; Hendricks Franssen et al., 1999; Gómez-Hernández et al., 2003; Drécourt et al., 2006; Hendricks Franssen and

Kinzelbach, 2008; Fu and Gómez-Hernández, 2009; Bailey and Baù, 2010). Several studies have employed three-dimensional steady-state flow models (Chen and Zhang, 2006; Liu et al., 2008), and several have estimated hydraulic parameters in variably-saturated flow conditions (Yeh and Zhang, 1996; Zhang and Yeh, 1997; Li and Yeh, 1999), although for the latter applications were limited to small 2-D vertical-plane systems. In general, however, critical components of hydrology in watershed systems, e.g., infiltration and percolation in variably-saturated porous media, ponding and overland flow, and stream channel flow have been neglected. Catchment models such as CATHY (CATchment HYdrology), based on the 3-D Richards equation for variably-saturated porous media and a diffusion wave approximation for overland and channel flow, have been used in data assimilation studies (Camporese et al., 2009, 2010), but not yet in parameter estimation. Estimation of parameters in land-surface models has been performed (e.g., Boulet et al., 2002; Xie and Zhang, 2010), although the models treat groundwater flow using simplified approaches.

In recognition that improved parameter estimation occurs when system-response data from more than one governing equation is used (Gailey et al., 1991), with the implication that each data type contains unique information regarding the parameter, numerous studies have employed two or more sets of dissimilar data to condition the parameter values. Such data sets typically include hydraulic head data as well as another data type such as solute concentration data (Gailey et al., 1991; Li and Yeh, 1999; Hendricks Franssen et al., 2003; Gómez-Hernández et al., 2003; Liu et al., 2008), groundwater temperature (Woodbury and Smith, 1988), groundwater travel time (Fu and Gómez-Hernández, 2009), groundwater discharge to surface water (Bailey and Baù, 2010), and tracer breakthrough data at observation wells (Wen et al., 2002). Streamflow data, which carries information regarding the spatial structure of aquifer K due to groundwater-surface water interactions, has been used in data assimilation to improve model performance (Schreider et al., 2001; Aubert et al., 2003; Clark et al., 2008; Camporese et al., 2009, 2010), although as yet has not been used to condition K.

1.2 Kalman Filter methods

In Kalman Filtering methods, a priori information, i.e., model parameters and associated model results, are merged with observation data from the true system to produce an a posteriori system estimate honoring the true system data at observation points, while still incorporating physically-based information from the numerical model. The resulting algorithm is used to merge model and measurement data whenever measurement data become available during the course of the model simulation.

In contrast to a filter, which assimilates data sequentially as they become available, a smoother incorporates all past model and measurement information in a single assimilation

step. The EnKF, EnKS, and ES all use an ensemble of realizations to represent numerically the measurement error statistics (Evensen, 2003), and are designed for large, nonlinear systems. The EKF, EnKF, EnKS, and ES have all been used in hydrologic modeling applications in both system-response updating (e.g., Schreider et al., 2001; Aubert et al., 2003; Dunne and Entakhabi, 2005; Clark et al., 2008; Durand et al., 2008; Camporese et al., 2009, 2010) and system parameter conditioning (Hantush and Mariño, 1997; Boulet et al., 2002; Chen and Zhang, 2006; Hendricks Franssen and Kinzelbach, 2008; Liu et al., 2008; Bailey and Baù, 2010; Xie and Zhang, 2010). Application of the EnKF and ES to highly nonlinear hydrologic systems such as a land surface model (Dunne and Entakhabi, 2005) and a coupled surface and variably-saturated subsurface flow model (Camporese et al., 2009) has proven successful.

1.3 Geostatistics in parameter estimation

Many parameter estimation studies employ geostatistical models (GMs) to define the a priori estimate of the spatial distribution of log-K or log-T (e.g., Kitanidis and Vomvoris, 1983; Hantush and Mariño, 1997; Chen and Zhang, 2006; Hendricks Franssen and Kinzelbach, 2008), under the assumption that aquifer K in regional systems can generally be described using such models (Kitanidis and Vomvoris, 1983; Hoeksema and Kitanidis, 1985; Carrera et al., 2005). The values of the parameter (e.g., log-K mean, log-K variance, correlation length) that characterize these GMs often have a strong influence on the response of a groundwater model and parameter estimation results (Jafarpour and Tarrahi, 2011), and yet in practice are estimated from limited geologic information and hence are not known with a high degree of certainty (Gautier and Nœtinger, 2004; Jafarpour and Tarrahi, 2011).

As a consequence, several methodologies have aimed at estimating the values of GM parameters, with the general approach of (i) performing "structural analysis", in which the form of the GM is selected, followed by (ii) an estimation of the values of the parameters defining the GM using observation data from the aquifer system. For example, Kitanidis and Vomvoris (1983) and Hoeksema and Kitanidis (1984) used maximum likelihood estimation to estimate values for a two-parameter GM using measurements of log-T and hydraulic head in 1-D and 2-D steady-state flow systems, respectively, in their approach to estimating the spatial distribution of log-T. A more recent review of the technique is given in Kitanidis (1996). More recent studies in the field of petroleum-reservoir engineering (e.g., Yortsos and Al-Afaleg, 1997; Gautier and Noetinger, 2004) have used well test data to estimate parameter values of the permeability variogram. For example, Gautier and Noetinger (2004) expanded on the work of Kitanidis and Vomvoris (1983) to develop a methodology for transient flow.

1.4 Objectives of this study

The objectives of this study are three-fold. The first objective is to apply the Kalman Filter parameter estimation methodology within a fully-coupled surface and variably-saturated subsurface flow model to provide more realistic simulation of water table elevation, as well as allow for streamflow to be simulated. To accomplish this, the CATHY model is used in a tilted v-catchment setting, similar in design to the v-catchment used by Camporese et al. (2009), with uncertain initial conditions (i.e., water table elevation) and uncertain patterns of applied water at the ground surface in space and time in a 365-day simulation. An ES is used to assimilate water table elevation data from a reference system to provide an updated estimate of the spatial distribution of log-K. Using uncertain initial conditions and forcing terms provides a stiff test for estimating K (Hendricks Franssen and Kinzelbach, 2008) since values of water table elevation and streamflow are not influenced solely by K. The second objective is to exploit the functionality of CATHY to explore the possibility of using streamflow measurements, solely and jointly with water table elevation data, to condition K.

The third objective is to use the ES in an iterative scheme to identify the parameters of a geostatistical model through assimilation of water table elevation data, and hence provide a new methodology for estimating the value of these parameters. In this study, the ability of the scheme to assess the log-mean and log-variance of a geostatistical model is investigated. Uncertainty in correlation scales is not addressed in this study, but is left to future work. Assessment of the true correlation scale for a given aquifer will likely require the direct assimilation of K measurements, whereas in this study only the model response variables are assimilated.

For the first and second objectives, the influence of the number of measurements and the uncertainty assigned the measurement data on the ability of the ES to provide accurate updates is investigated. Overall, with uncertainty in initial conditions, forcing terms, and geostatistical model parameters, the complexity of real-world systems is approached, providing a key liaison between theory and real-world application.

2 Methodology

In this section, the theoretical development of the ES update algorithm is presented within the context of estimating the spatial distribution of K using observed water table elevation (WT) and streamflow (Q) data from a reference catchment system. The general forecast and update steps of the Kalman Filter are first discussed, followed by a modification of these steps for the ES scheme.

2.1 Forecast of system state

Using an ensemble of n_{MC} system realizations to establish the uncertainty in the system, the state of the system is estimated using the *model forecast* step:

$$X_t^f = \Phi_t(\boldsymbol{P}; \boldsymbol{X}_0; \boldsymbol{q}; \boldsymbol{b}) \tag{1}$$

where f indicates *forecast*, $\boldsymbol{X}_t^f$ contains the ensemble of re-alizations of the forecasted estimate of the system at time t, Φ_t represents the solution to the numerical model, and $\boldsymbol{P}$, $\boldsymbol{X}_0$, $\boldsymbol{q}$, and $\boldsymbol{b}$ represent the system parameters, initial conditions, forcing terms, and boundary conditions, respectively. The numerical model employed in this study is the CATHY model, and is used to generate values of WT and Q as well as establish relationships between the system parameter (i.e., K) and the system response variables (i.e., WT and Q).

CATHY simulates subsurface, overland, and channel flow by coupling the 3-D Richards equation for variably satu-rated porous media with a 1-D diffusion wave approxima-tion of the de Saint Venant equation for surface flow (Bixio et al., 2000; Camporese et al., 2010). The groundwater flow equation is given by Camporese et al. (2010):

$$S_w S_s \frac{\partial \psi}{\partial t} + \varphi \frac{\partial S_w}{\partial t} = \nabla \cdot [\boldsymbol{K}_s K_r (\nabla \psi + \eta_z)] + q_{ss} \tag{2a}$$

where $S_w = \theta/\theta_s$, with θ and θ_s as volumetric water content [-] and saturated water content (porosity) [-], respectively, S_S is the specific storage coefficient [L^{-1}], ψ is pressure head [L], t is time [T], ∇ is the spatial gradient operator [L^{-1}], $\boldsymbol{K}_s$ is the saturated hydraulic conductivity tensor [LT^{-1}] with $\boldsymbol{K}_s$ treated as a scalar field when conditions of isotropy are hypothesized, $K_r(\psi)$ is the relative hydraulic conductivity function [-], $\eta_z = (0, 0, 1)$, z is the vertical coordinate di-rected upward [L], and q_{ss} represents distributed source or sink terms [$L^3 L^{-3} T^{-1}$].

Using a 1-D coordinate system s [L] to describe the chan-nel network, the surface water flow equation is given by (Camporese et al., 2010):

$$\frac{\partial Q}{\partial t} + c_k \frac{\partial Q}{\partial s} = D_h \frac{\partial^2 Q}{\partial s^2} + c_k q_s \tag{2b}$$

where Q is the discharge along the stream channel [$L^3 T^{-1}$], c_k is the kinematic celerity [LT^{-1}], D_h is the hydraulic diffu-sivity [$L^2 T^{-1}$], and q_s is the inflow or outflow rate from the subsurface to the surface [$L^3 L^{-1} T^{-1}$].

In CATHY, Eq. (2a) is solved using Galerkin finite el-ements (FE), whereas Eq. (2b) is solved using an explicit time discretization based on the Muskingum-Cunge rout-ing scheme (Orlandini and Rosso, 1996). In this study, the $K_r(\psi)$ and $S_w(\psi)$ relationships are specified using the for-mulation of van Genuchten and Nielsen (1985), although other capillary curves are available in CATHY (see Cam-porese et al., 2010). The channel network is identified us-ing the terrain topography from a digital elevation model
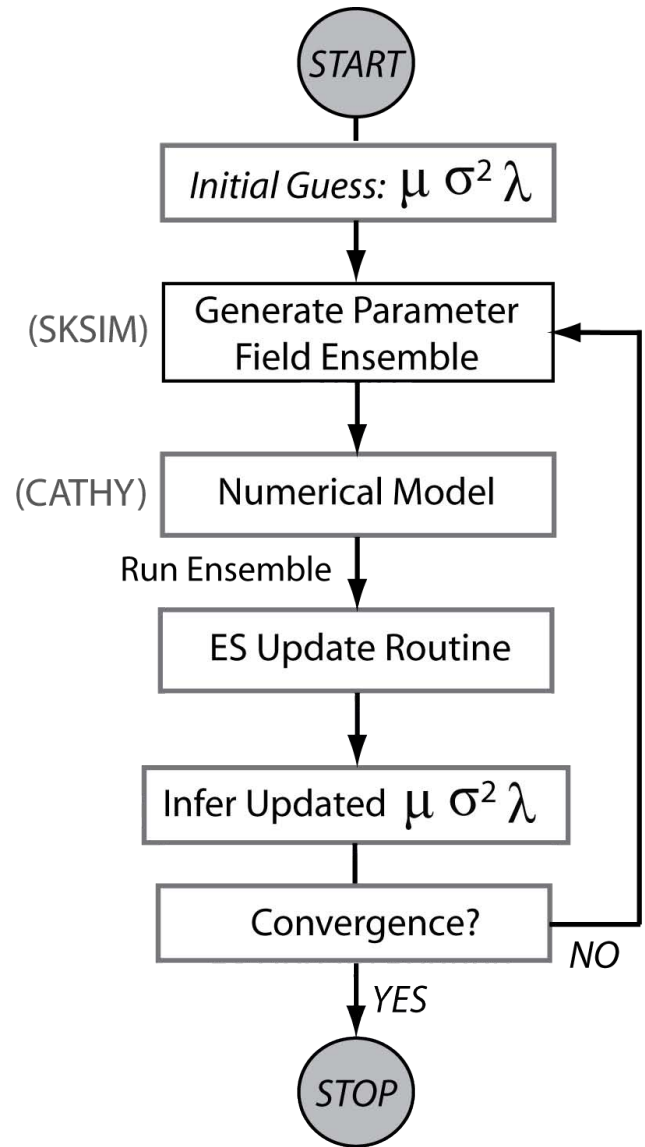

Fig. 1. Flow chart for the iterative approach using an Ensemble Smoother to estimate geostatistical values.

(DEM) and the hydraulic geometry concept used by Orlan-dini and Rosso (1996). The DEM cells are then triangulated to generate a 2-D triangular FE mesh, which is replicated vertically to construct a 3-D tetrahedral FE mesh for the subsurface system. Interaction between surface water and groundwater modeled in CATHY is described by Putti and Paniconi (2004).

As will be discussed further in Sect. 2.2, the resulting sys-tem state $\boldsymbol{X}$ (Eq. 1) is comprised of: (1) a WT value for each node of the triangular FE mesh, calculated using the verti-cal profile of ψ for each of these nodes; (2) a K value for each DEM cell in the horizontal direction; (3) a Q value for each DEM grid cell along a stream channel. If e and n de-note the number of DEM cells and FE nodes in the horizontal
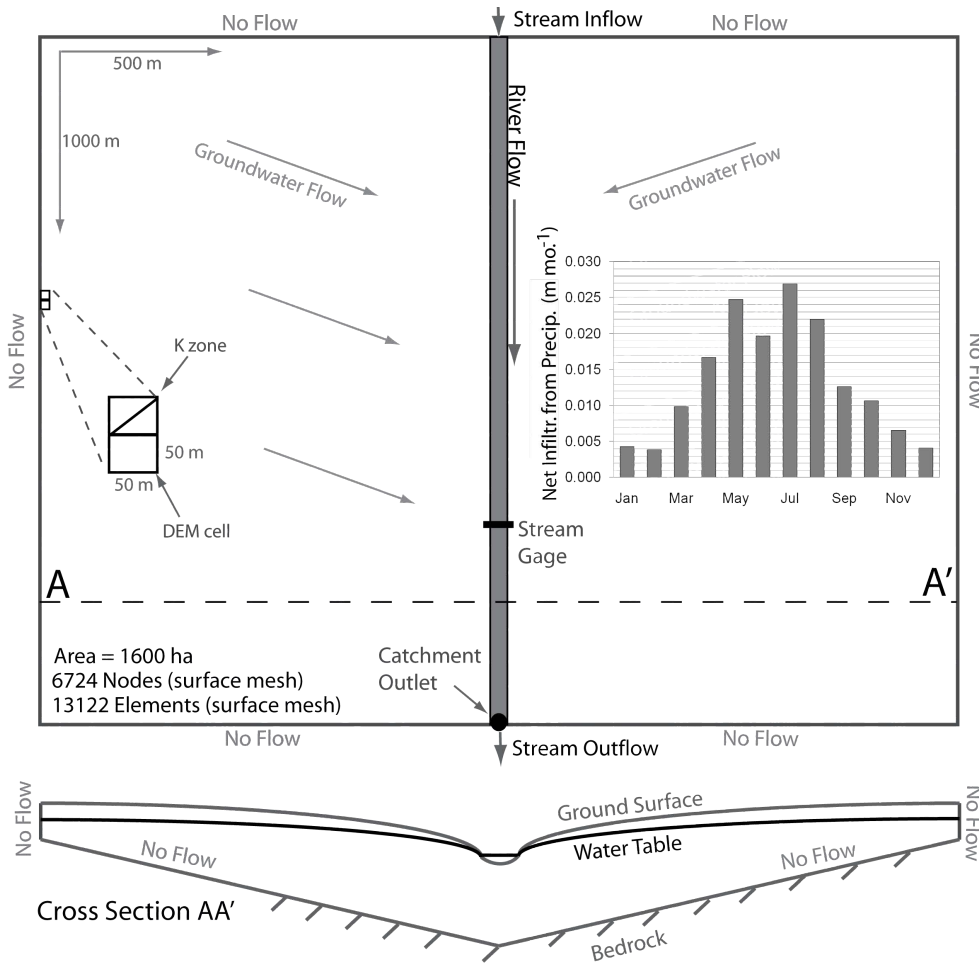
Fig. 2. Conceptual model of tilted v basin through the catchment outlet. The monthly depth of -shaped catchment, with groundwater feeding the river flowing out of the net infiltration from precipitation is also shown.

direction, respectively, and g the number of DEM cells along the stream channel, then the dimension d of X is equal to $[n + e + g]$. The forcing terms q in Eq. (1) are represented by q_{ss} in Eq. (2a), and in this study correspond to rates of applied water at the ground surface, with uncertainty established by sampling values from a prescribed frequency distribution. Uncertainty in X_0 is also included, as discussed in Sect. 3.1.

The spatially-variable values of $Y_K = \log K$ are generated using SKSIM (Baù and Mayer, 2008), a sequential Gaussian simulation algorithm, where the spatial distribution and correlation is established by a normal distribution wherein the geostatistical model is a 2-D exponential covariance model in the logarithmic domain:

$$\log K = Y_K = N\left(\mu_{Y_K}; \sigma_{Y_K}\right)$$

$$\mathrm{cov}_{Y_K, Y_K}(d) = \sigma_{Y_K}^2 \cdot \exp\left(\sqrt{\sum_{i=1}^{2} \frac{d_i^2}{\lambda_i^2}}\right) \tag{3}$$

where μ_{Y_K} and σ_{Y_K}, and $\sigma_{Y_K}^2$ are the mean, standard deviation, and variance of the logarithmic distribution of the parameters, respectively, d_is are the components of the distance vector d, and λ_is are the spatial correlation scales in the coordinate directions.

2.2 Update of system state

Correction to the a priori estimate X_t^f is accomplished by assimilating observed system-response data from the true system, thereby merging the model-calculated and observed values. This correction depends on the uncertainty attached to both the a priori estimate (i.e., the model results) and the true values (i.e., the observations from the true system), with uncertainty in the model forecast provided by the spread in the ensemble values and uncertainty in the observed values specified according to data-sampling methods. The correction made to the model-calculated values by the observed values is dictated by the ratio of these uncertainties. If there is less
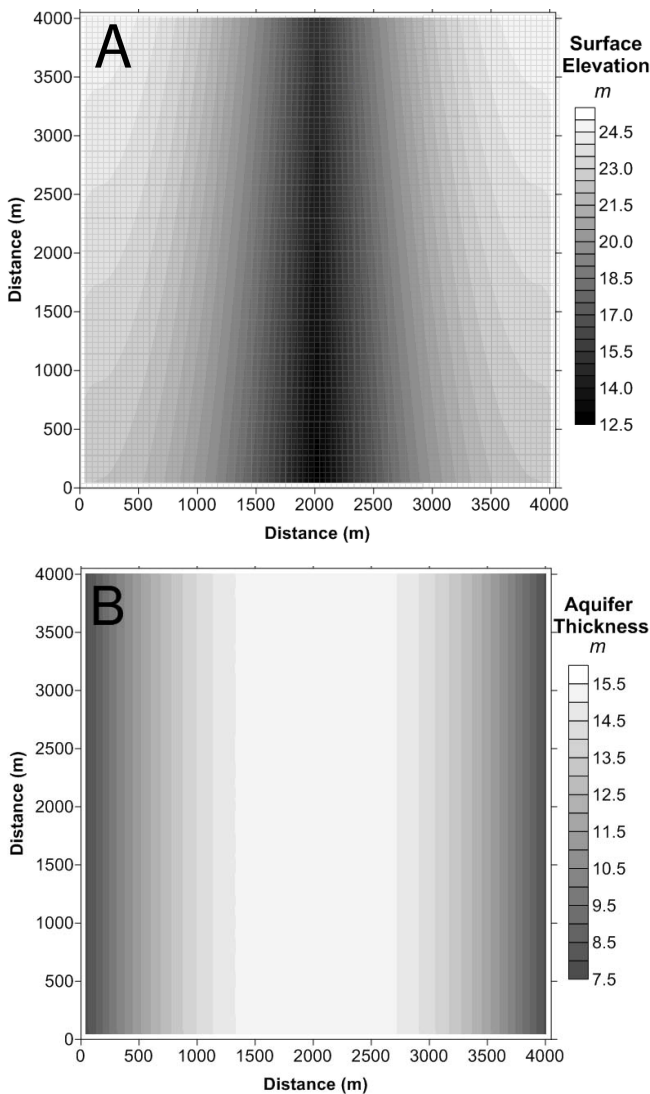
Fig. 3. Contour representation of **(A)** ground surface elevation and **(B)** aquifer thickness. Both datasets are used to create the three-dimensional subsurface finite-element mesh.

Table 1. Frequency distribution of the ensemble of perturbed values for the observed WT value of 18.5 m collected on day 91 at location (X = 2500 m, Y = 3500 m) of the "true aquifer", for CV values of 0.10 and 0.30.

DEM Attributes	
Cells in x direction	81
Cells in y direction	81
Grid spacing m	50
Number of cells	6561

Mesh Attributes	
Aquifer Thickness	7.5 to 15.5
Number of Layers	10
Number of Surface Nodes	6724
Number of 3-D Mesh Nodes	73 964
Number of Tetrahedral Elements	393 660

System Parameters	
Saturated hydraulic conductivity K_s	GM: Eq. (3)
Mean μ of K fields	log 1.30 (m d^{-1})
Variance σ^2 of K fields	log 0.25 (m d^{-1})^2
Correlation Length λ of K fields	1000 m
Specific storage S_s	0.01 m^{-1}
Porosity n	0.35
Residual moisture content θ_r	0.061
van Genuchten parameters	$\alpha = 0.43\,\mathrm{m}^{-1}$, $n = 1.70$

Simulation details	
Monte Carlo Ensemble Size	100
Simulation period $days$	730.0

uncertainty attached to the observed data, which is typically the case, then the model-calculated value at the observation location will be corrected to approach the observed value. Furthermore, model results can also receive correction from observed data if the model value is correlated with the model value at the observation location. In this way information from the true state at observation points can be "spread" to regions between observation locations, and hence throughout the model domain.

This correction procedure is carried out through the following Kalman Filter update equation, with the forecasted ensemble X_t^f corrected, or updated, at a time t using m observed data stored in a vector M_t [m]:

$$X_t^u = X_t^f + \kappa_t \left(\mathbf{D}_t - \mathbf{H}\mathbf{X}_t^f \right) \tag{4}$$

where $X_t^u [dxn_{\mathrm{MC}}]$ is the updated ensemble with u denoting update; $\mathbf{D}_t$ [mxn_{MC}] holds the ensemble of perturbed values of the measurement data, with the ensemble of values for each measurement value calculated by adding a Guassian perturbation (stored in the matrix $\mathbf{E}$ [mxn_{MC}]) to each of the m observations stored in M_t; H [mxd] contains binary constants (0 or 1) resulting in the matrix product $\mathbf{H}\mathbf{X}_t^f$ that holds model results at measurement locations, and κ_t [dxm] is the so-called "Kalman Gain" matrix. In this study, observation data are sampled from a known reference state to enable assessment of the ES scheme.

In Eq. (4), the difference, or residual, between the model values and observed values is represented by $\left(\mathbf{D}_t - \mathbf{H}\mathbf{X}_t^f \right)$, with the weighting of the correction and the spatial spread of the information dictated by κ_t, which holds the ratio of uncertainties as well as the covariance between model values at each model node (Bailey and Baù, 2011). The form of
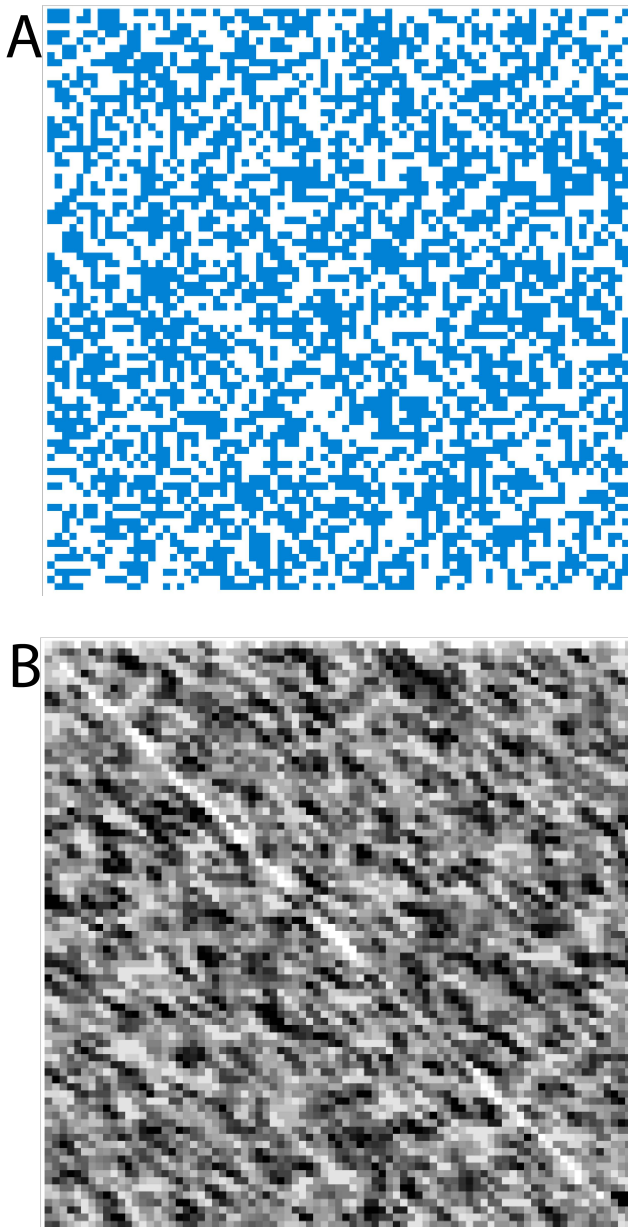
Fig. 4. **(A)** Cultivated (blue) and non-cultivated fields (white), with cultivated fields receiving additional applied water during the months of April through October, and **(B)** Net infiltration in the month of July (of the second year) for the true system, with values ranging from 0.000355 m day^{-1} to 0.006 m day^{-1} (represented by white and black, respectively).

κ_t is:

$$\kappa = \mathbf{C}^f \mathbf{H}^T \left(\mathbf{H} \mathbf{C}^f \mathbf{H}^T + \mathbf{R} \right)^{-1} \quad (5)$$

where $\mathbf{C}^f$ [$d \times d$] and $\mathbf{R}$ [$m \times m$] are the forecast error and observation error covariance matrices, respectively, and are
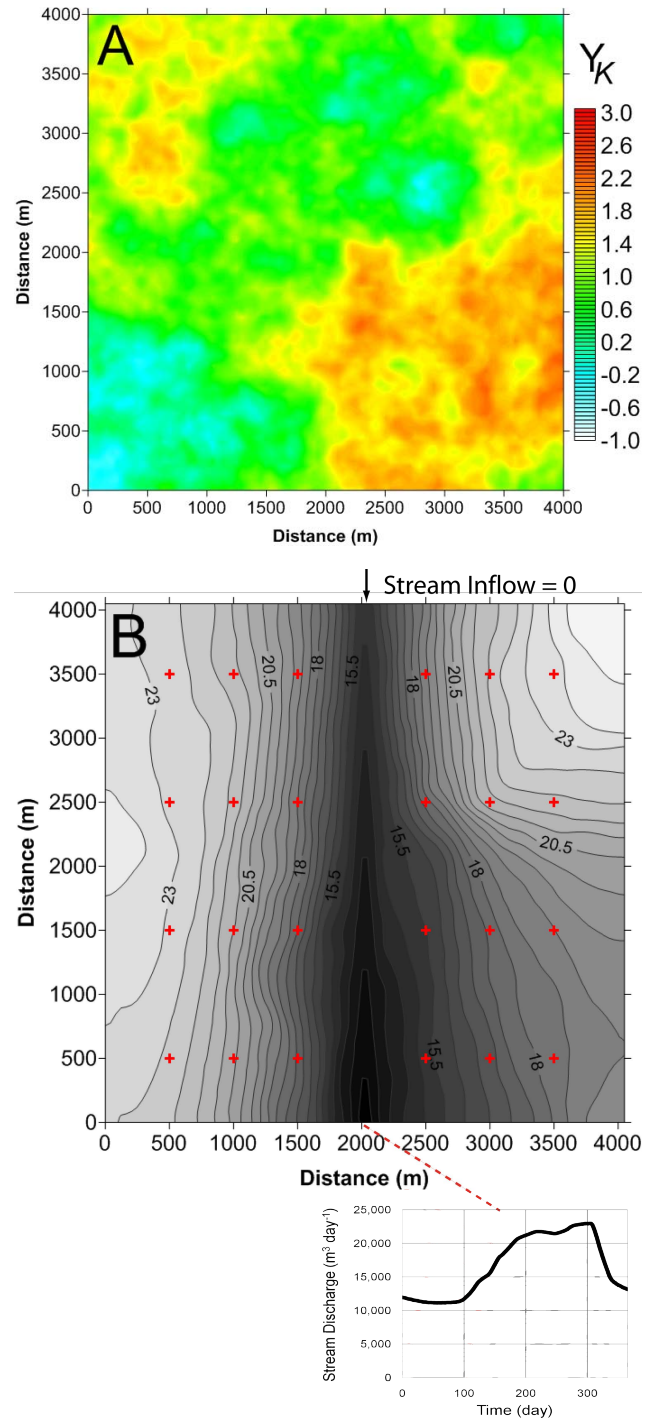

Fig. 5. **(A)** Reference field of true Y_K and **(B)** corresponding WT field at time = 365 days as calculated by CATHY. In **(B)**, red crosses indicate the location of 24 observation wells. The streamflow at the outlet cell during the 365-day simulation is shown in the subpanel.

defined as:

$$\mathbf{C}^f = \frac{\left(X_{t+\Delta t}^f - \overline{X} \right) \left(X_{t+\Delta t}^f - \overline{X} \right)^T}{nmc - 1} \quad (6a)$$

$$\mathbf{R} = \frac{E E^T}{nmc - 1} \tag{6b}$$

where each column of $\overline{X}[n \text{ x } n_{\mathrm{MC}}]$ holds the average value of the ensemble at each location in the domain.

In a straightforward application of data assimilation to a catchment system, Eq. (4) would correspond to merging observed values of WT (or Q) with the model-calculated WT field (or Q along a stream channel) in order to provide a WT field that honors the observed WT data. However, doing so only corrects the system response of the model – the structural difference between the a priori model state and the true state that yields differences in the system response will persist indefinitely. To temper these structural differences, it is essential to correct the parameters that drive the system response. This can be accomplished by utilizing the relationships between K and the resulting values of WT and Q as established through CATHY. For example, the cross-covariance submatrix between WT and Y_K is defined as:

$$\mathbf{C}_t^f \left(X_{(WT)}, X_{(Y_K)} \right) = \frac{\left[\left(X_t^f - \overline{X} \right)_{WT} \right] \left[\left(X_t^f - \overline{X} \right)_{Y_K} \right]^T}{n_{\mathrm{MC}} - 1} \tag{7}$$

By including the expression for Eq. (7) into Eq. (5), the values of Y_K in X_t^f can be corrected by observation data in D_t through the spatial correlation between Y_K, WT, and Q.

2.3 Forecast-Update scheme for the ensemble smoother

Whereas Eqs. (1) and (4) are run in a sequential manner in the KF and EnKF schemes, with correction via Eq. (4) occurring whenever observation data are sampled from the true system, the ES algorithm includes all previous model state and observation data up to the final data sampling time t_{nF}, at which time the ES update routine is run to provide updated system states at all previous collection times. At time t_{nF}, the forecast matrix $\widetilde{X}_{t_F}^f$ and the observation matrix $\widetilde{D}_{t_F}$ hold the model state ensembles and the perturbed observation data from all data sampling times $(t_1, t_2, \ldots, t_{nF})$:

$$\widetilde{X}_{t_F}^f = \left[X_{t_1}, X_{t_2}, \ldots, X_{t_{nF}} \right]^T [(d)\,(nF)] \mathrm{x} n_{\mathrm{MC}} \tag{8a}$$

$$\widetilde{D}_{t_f} = \left[D_{t_1}, D_{t_2}, \ldots, D_{t_{nF}} \right]^T [(m)\,(nF)] \mathrm{x} n_{\mathrm{MC}} \tag{8b}$$

where nF is the number of times at which measurements are collected. Within the ES scheme, the forecast covariance matrix $\widetilde{C}_{t_{nF}}^f$ contains both spatial covariance terms and temporal covariance terms between cell values from different collection times (*Evensen*, 2007). The measurement error covariance matrix $\widetilde{R}_{t_{nF}}$ also is established using the perturbations for each of the measurement values for each of the nF collection times. By inserting $\widetilde{X}_{t_{nF}}^f$ and $\widetilde{D}_{t_{nF}}$ into Eq. (4) and $\widetilde{C}_{t_{nF}}^f$
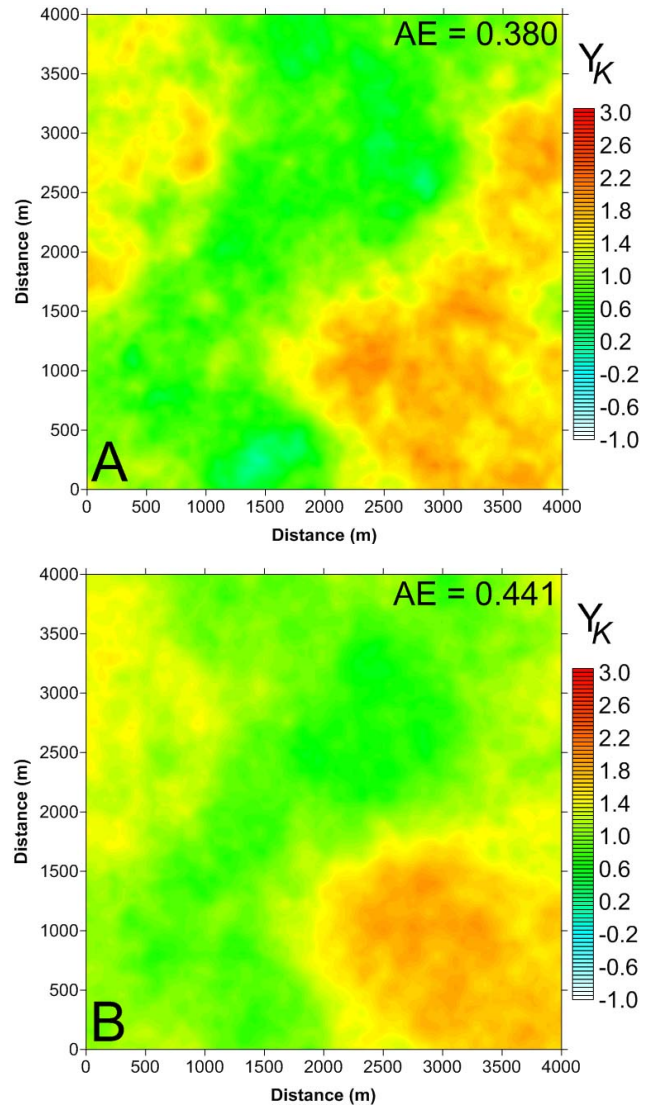

Fig. 6. Spatial distribution of the updated Y_K ensemble using data from 24 observation wells sampled 4 times during the 365-day period, with the CV of observation data set to **(A)** 0.0 and **(B)** 0.3. Compare to the true state shown in Figure 5A.

and $\widetilde{R}_{t_{nF}}$ into Eq. (5), the updated system state matrix $\widetilde{X}_{t_{nF}}^u$ contains the updated model state for each assimilation time.

The Keppenne (2000) algorithm, which provides an efficient numerical strategy for updating the system state for the EnKF scheme and designed for high-resolution real-world climate numerical models, was modified to include model states and observation data from each assimilation time (Bailey and Baù, 2010) and used to compute Eq. (4) within the ES framework. The techniques employed by Keppenne (2000) and hence inherent in the update algorithm used in this study do not require the direct assemblage of C^f, hence saving on computer memory and preventing numerical issues.

Table 2. The increase of AE (i.e., the decrease in conditioning to the true Y_K field) with increasing values of CV of the WT observation data, for the cases when one, two, and four assimilation times are used.

Scenario	Num Gage Q	Num AT Q	CV Q	AE K	% Reduct	AEP K	% Reduct
FORECAST	–	–	–	0.619	–	0.388	–
UPDATE							
1	4	4	0.00	0.512	17.3 %	0.305	21.3 %
2	4	4	0.10	0.574	7.3 %	0.368	5.0 %
3	4	4	0.30	0.607	2.0 %	0.384	1.0 %
4	4	4	0.50	0.614	0.9 %	0.386	0.4 %
5	4	4	0.70	0.616	0.5 %	0.387	0.2 %
6	4	4	1.00	0.617	0.3 %	0.387	0.1 %

Table 3. Spatial distribution of the mean of the updated Y_K ensemble using Y_Q data from four gaging stations along the stream channel sampled four times during the 365-day period, with the CV of observation data set to 0.0. Compare to the true state shown in Fig. 5a.

Scenario	Num Assim Var	Num Meas WT	Num Gage Q	Num AT WT	AT Q	CV WT	CV Q	AE Y_K	% Reduct	AEP Y_K	% Reduct
FORECAST								0.619	–	0.388	–
UPDATE											
1		24	0	4	–	0.00	–	0.380	38.6 %	0.203	47.7 %
2		8	0	4	–	0.00	–	0.447	27.8 %	0.261	32.6 %
3	WT	4	0	4	–	0.00	–	0.455	26.4 %	0.297	23.3 %
4		2	0	4	–	0.00	–	0.545	11.9 %	0.334	13.9 %
5		24	4	4	4	0.00	0.00	0.380	38.6 %	0.203	47.7 %
6		8	4	4	4	0.00	0.00	0.440	29.0 %	0.252	35.0 %
7	WT, Q	4	4	4	4	0.00	0.00	0.434	29.9 %	0.284	26.9 %
8		2	4	4	4	0.00	0.00	0.482	22.1 %	0.301	22.3 %

2.4 Evaluating the updated system state

The ability of the ES algorithm to bring the forecasted ensemble into conformity with the true system state is quantified through two location-specific parameters *EE* (ensemble error) and *EP* (ensemble precision) and two global parameters *AE* (absolute error) and *AEP* (average ensemble precision) (Hendricks Franssen and Kinzelbach, 2008; Bailey and Baù, 2011):

$$EE_i = \left| \overline{X}_i - X_{i,true} \right| (i = 1, \ldots, n) \tag{9a}$$

$$EP_i = \frac{1}{nmc} \sum_{j=1}^{nmc} \left| X_{i,j} - \overline{X}_i \right| (i = 1, \ldots, n) \tag{9b}$$

$$AE(X) = \frac{1}{(nmc)(n)} \sum_{j=1}^{nmc} \sum_{i=1}^{n} \left| X_{i,j} - X_{i,\text{true}} \right| \tag{9c}$$

$$AEP(X) = \frac{1}{(nmc)(n)} \sum_{j=1}^{nmc} \sum_{i=1}^{n} \left| X_{i,j} - \overline{X}_i \right| \tag{9d}$$

where $\overline{X}_i$ is the ensemble mean of the ith location (node in a FE discretization of the domain or cell of the surface DEM grid), $X_{i,\text{true}}$ is the reference "true" value of the ith location, and $X_{i,j}$ is the variable value of the i location of the jth ensemble realization. Equation (9a) and (c) provide a measure of the deviation between the model state and the reference state, and Eq. (9b) and (d) provide a measure of the spread of the values around the ensemble mean of the model state. The performance of the update routine is measured by calculating the difference between performance parameters of the forecasted and updated ensembles. As a second type of performance measure, the ensemble of CATHY simulations can be rerun using the updated ensemble of Y_K fields to determine if the updated Y_K ensemble produces simulated

www.hydrol-earth-syst-sci.net/16/287/2012/

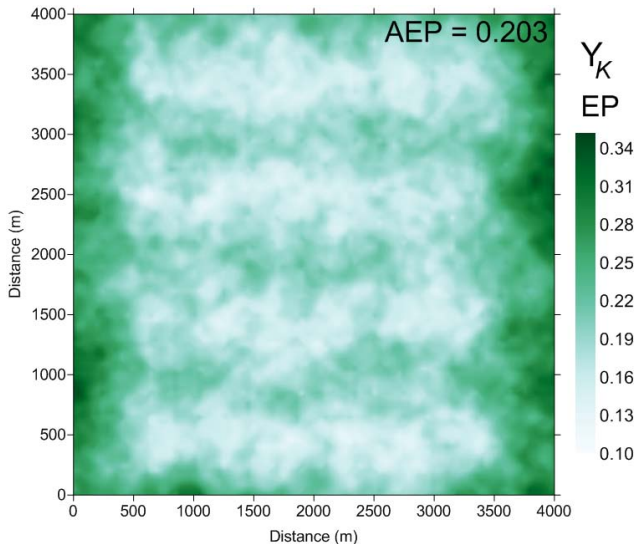Hydrol. Earth Syst. Sci., 16, 287–304, 2012

Fig. 7. Spatial distribution of EP for the updated Y_K ensemble using data from 24 observation wells sampled 4 times during the 365-day period, with the CV of observation data set to 0.0.
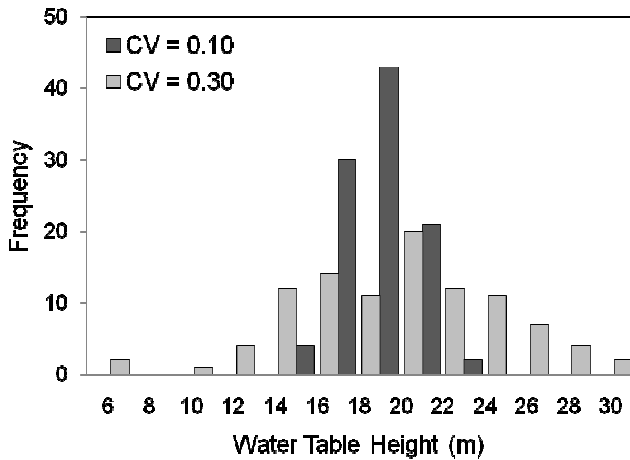

Fig. 8. Frequency distribution of the ensemble of perturbed values for the observed WT value of 18.5 m collected on day 91 at location (X = 2500 m, Y = 3500 m) of the "true aquifer", for CV values of 0.10 and 0.30.

results that match the observed data, i.e., to see if the model has been "calibrated" adequately. This latter method will be demonstrated in Sect. 3.3.2.

2.5   Iterative method to estimate geostatistical parameters

In the forecast step of Sect. 2.1, it is assumed that the parameters defining the GM of Eq. (3) are known, i.e., that the parameter values used to generate the ensemble of Y_K fields for the forecast simulations are the same as the reference system from which the observation data is sampled. In recognition
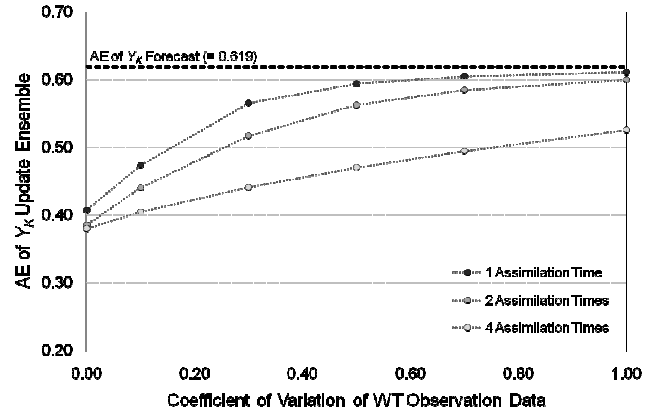

Fig. 9. The increase of AE (i.e., the decrease in conditioning to the true Y_K field) with increasing values of CV of the WT observation data, for the cases when one, two, and four assimilation times are used.
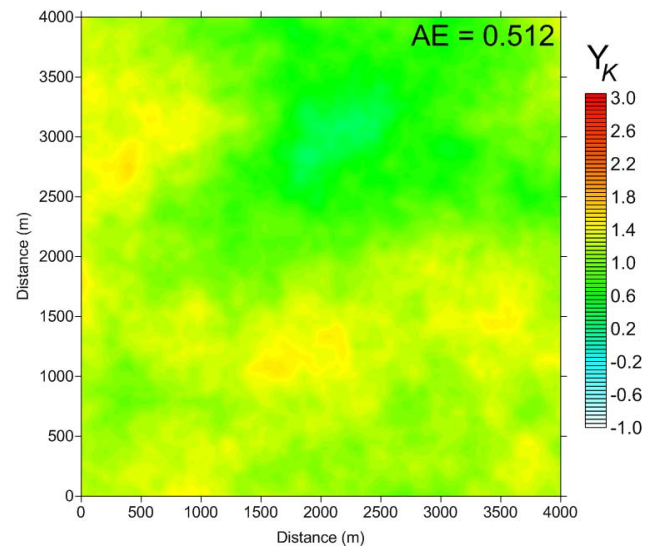

Fig. 10. Spatial distribution of the mean of the updated Y_K ensemble using Y_Q data from four gaging stations along the stream channel sampled four times during the 365-day period, with the CV of observation data set to 0.0. Compare to the true state shown in Fig. 5a.

that this is generally not the case, the ES scheme decribed in Sect. 2.1 through Sect. 2.3 is employed in an iterative scheme to discover the geostatistical parameter values of the true system, as shown in Fig. 1. Beginning with a set of estimated GM parameter values, an ensemble of Y_K fields is generated using SKSIM and the corresponding ensemble of CATHY flow simulations is run. Upon assimilating observation data from the reference system and conditioning the Y_K ensemble, the GM parameter values of the updated Y_K ensemble are inferred from the updated ensemble and used to produce the forecast Y_K ensemble for the subsequent iteration. This

process proceeds until GM parameter values are converged upon. At each iteration the model-calculated values of WT can also be compared to the observed WT data from the true aquifer system, to verify that the estimated GM parameter values from the previous iteration yield a spatial structure of Y_K that furnishes the system response of the true system. It should be noted that estimation of the correlation scale λ was not pursued extensively in this study, as it became evident during initial uses of the iterative approach that λ could not be estimated using only a model-response variable such as water table elevation. As discussed in Sect. 4, the direct assimilation of Y_K values are likely required to provide information regarding λ, and will be pursued in future work.

3 Parameter Estimation of Spatially-Variable K

3.1 Forecast ensemble of K, WT, and Q

The catchment system used for the numerical experiment in this study is a 4.05 km by 4.05 km tilted v-shaped catchment, as shown in Fig. 2, with a stream flowing north to south along the central depression of the catchment. The DEM of the surface terrain, discretized using 50 m by 50 m grid cells for a total of $e = 81 \times 81 = 6561$ grid cells, is shown in Fig. 3a with a contour plot of the ground surface elevation. Aquifer thickness varies between 7.5 m and 15.5 m, with the thickest portion under the central depression, as shown in Figs. 2 and 3b. The subsurface is discretized by $n_L = 10$ layers of varying thickness, with thicknesses ranging from 0.375 m near the ground surface to 3.0 m near the aquifer base.

The characteristics of the DEM, the 3-D mesh, and the parameters of the model are summarized in Table 1. The number of nodes in the 2-D surface FE mesh is $n = 82 \times 82 = 6724$. The 3-D mesh is obtained from replicating the 2-D FE mesh through the vertical extent of the subsurface and contains $3 \times n_L \times 2e = 393\,660$ tetrahedral elements and $n \times (n_L + 1) = 73\,964$ nodes. Lateral spatial distribution of Y_K for the forecast ensemble is generated using mean $\mu_{Y_K} = 1.301$ log m day^{-1} ($K = 20$ m day^{-1}), standard deviation $\sigma_{Y_K}^2 = (0.250$ log m day$^{-1})^2$, and correlation length $(\lambda_x = \lambda_y) = 1000$ m, resulting in K values ranging from approximately 0.2 m day^{-1} to 1500 m day^{-1}. In this study, $n_{\text{MC}} = 100$ realizations are used for the ensemble. Values of Y_K are calculated for each DEM cell, resulting in a value of Y_K assigned to each 3-D FE under the cell. In other words, the spatial distribution of Y_K is the same for each of the 10 layers in the 3-D mesh. Vertical hydraulic conductivity, K_v, is set equal to one-third the value of horizontal K.

The simulation period is one year, from January to December. No-flow boundaries are assigned for every edge of the aquifer (see Fig. 2). Forcing terms q_{ss} consist of uniformly-distributed net infiltration from precipitation during the months of January through March and November through December, and spatially-varying rates of net infiltra-

tion from applied water (e.g., irrigation water) in addition to net infiltration from precipitation during the months of April through October. For the latter, rates are applied according to the cultivation pattern depicted in Fig. 4a, with cells shown in blue receiving monthly values randomly sampled from an exponential distribution (rate parameter $\gamma = 0.75$). The pattern of cultivation shown in Fig. 4a is the same for each realization, but monthly rates vary across the realizations. The resulting rates are not intended to represent particular irrigation practices, but rather to provide a spatio-temporal variation in the forcing terms of the catchment system. As an example, the rates of net infiltration from combined precipitation and applied water for the month of July for one realization are shown in Fig. 4b, with values ranging from 0.000355 m day^{-1} to 0.006 m day^{-1} (represented by white and black, respectively). The depth of monthly net infiltration is presented in Fig. 2.

Initial conditions for each simulation are achieved as follows. First, a 10 000-day spin-up simulation with a uniform net infiltration rate of 0.0012 m day^{-1} and isotropic, homogeneous aquifer with $K = 30$ m day^{-1} is run in order to achieve steady-state conditions in the catchment as determined by water table elevation and streamflow rate. Second, each realization of the ensemble is run for 365 days using a different anisotropic Y_K field and infiltration pattern to eliminate the bias due to the initial conditions. The results of this 365-day simulation are then used as initial conditions for the final 365-day simulation period for each realization, with time steps ranging between approximately 0.10 to 1.0 day. Stream inflow (Fig. 2) is set to 0.

An additional CATHY simulation representing the true catchment system is run, with the true Y_K field and resulting true WT field (at 365 days) depicted in Fig. 5. The streamflow rate at the outlet cell of the catchment is shown in Fig. 5b, indicating the increased discharge during the months of April through October due to increased rates of net infiltration from precipitation as well as applied water. In comparing the Y_K forecast ensemble to the true Y_K field using Eq. (9c) and (d), the AE and AEP values are 0.619 and 0.388, respectively.

The GM parameter values used to generate the Y_K field are the same as used for the forecast ensemble. This assumption will be relaxed in Sect. 3.3.2, when the iterative approach presented in Sect. 2.5 is used to estimate the true GM parameter values. The ability of the ES scheme to recover the spatial distribution of the true Y_K field by assimilating WT and Q measurements into the forecast ensemble results is explored in Sect. 3.2.

WT data and Q data are collected from observation wells (Fig. 5b) and stream gaging points (Fig. 2), respectively. CPU (Central Processing Unit) time to run a single realization on an Intel® Core™2 Duo CPU @ 3.00 GHz desktop computer range from approximately 20 min to 180 min, depending on the spatial distribution of Y_K.
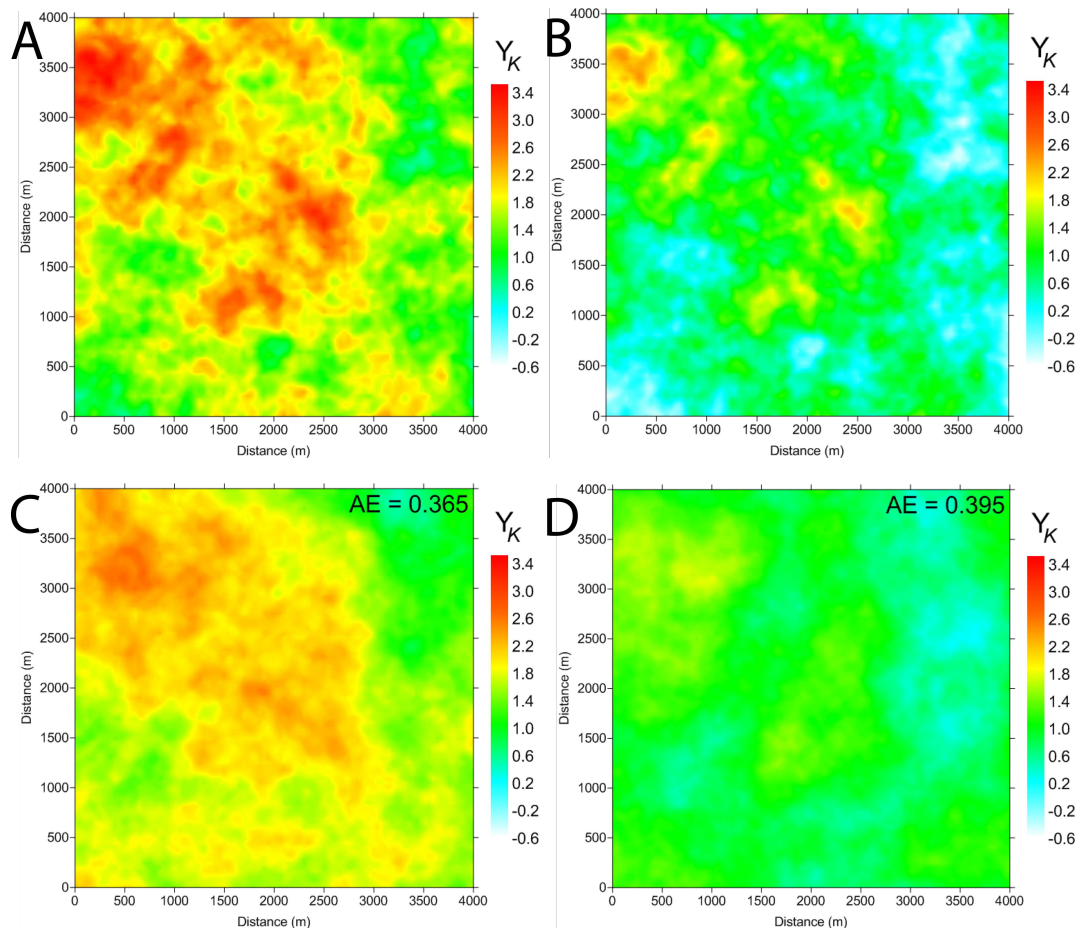
Fig. 11. (A) True Y_K field using $\mu_{y_K} = 1.801$ log m day^{-1} ($K = 63.2$ m day-1), **(B)** True Y_K field using $\mu_{y_K} = 0.801$ log m day^{-1} ($K = 6.3$ m day-1), **(C)** mean distribution of the updated Y_K ensemble for the first scenario ($\mu_{y_K} = 1.801$), and **(D)** mean distribution of the updated Y_K ensemble for the second scenario ($\mu_{y_K} = 0.801$). For both scenarios scenario, 24 WT data from four assimilation times are used.

3.2   Update of K ensemble

Observation data from the true catchment system are collected tri-monthly, resulting in four assimilation times during the year. As such, forecast ensemble model results are also saved every three months for use in the ES algorithm. The first set of update scenarios consists of conditioning the forecast Y_K ensemble using WT data from the 24 observation wells shown in Fig. 5b, with variations on (i) the number of assimilation times and (ii) the error, defined using coefficient of variation (CV) of WT data, assigned to the observed WT data. For these scenarios, the CPU run-time of the ES update routine is approximately 30 s.

For the scenario where four assimilation times are used and the observation data are assumed to be error-free, the ensemble mean at each computational point for the updated Y_K ensemble is shown in Fig. 6a. The AE value of the updated Y_K ensemble, measuring the absolute error from the true Y_K field, is 0.380, a reduction of 38.6 % from the forecast value of 0.619. In comparison with the true Y_K field

shown in Fig. 5a, the mean of the updated Y_K ensemble in Fig. 6a captures the overall spatial pattern of the true field, with high values of Y_K in the northwest and southeast sections of the aquifer and low values in the north-central and southwest portions. The updated AEP value, measuring the spread of the updated Y_K ensemble, is 0.203, a reduction of 47.7 % from the forecast value of 0.388. The spatial distribution of EP for the updated Y_K ensemble, as calculated by Eq. (9b), is shown in Fig. 7. Notice that the spread of the ensemble values is lowest at and around the locations of the 24 observation wells.

When a CV value of 0.10 is assigned to the WT observation data, the AE and AEP values of the updated Y_K ensemble are 0.405 and 0.246, respectively, reductions of 34.5 % and 36.6 % from the forecast values. When a CV value of 0.30 is assigned, the AE and AEP values are 0.441 and 0.284, reductions of 28.8 % and 26.8 % from the forecast values. The ensemble of perturbed values for a data value collected from the observation well located at location (X = 2500 m, Y = 3500 m) for these two cases is shown in Fig. 8. For the
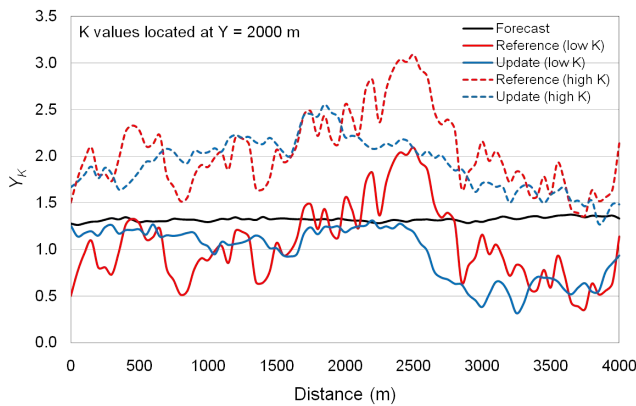
Fig. 12. Comparison of reference and updated values of Y_K along the $Y = 2000$ m transect where the true is higher (1.801 log m day^{-1}) and lower (0.801 log m day^{-1}) than the of the forecast ensemble (1.301 log m day^{-1}). The values from the reference state are shown in red, and the updated values are shown in blue. For both scenarios, 24 WT measurements are assimilated.
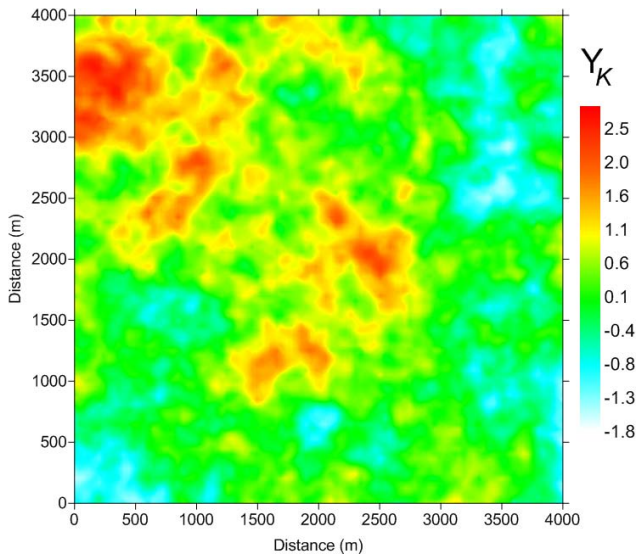

Fig. 13. Reference Y_K field with $= 0.301$ log m day^{-1} (2.0 m day^{-1}) and $= 0.500$ (log m day^{-1})^2.

latter case, the ensemble mean of the updated Y_K ensemble is shown in Fig. 6b. In comparison to the case of CV = 0.00 (Fig. 6a), the spatial distribution of Y_K does not resemble as well the true Y_K field shown in Fig. 5a.

When observation data from only one assimilation time (time = 365 days) is assimilated, the AE value of the updated Y_K ensemble is 0.408; when observation data from two assimilation times are used (time = 181 days and 365 days), the AE value is 0.385. In comparison to the AE value of 0.380, when four assimilation times are used, the improvement of the updated Y_K ensemble with respect to the true Y_K field is not considerable. The usefulness of additional assimilation
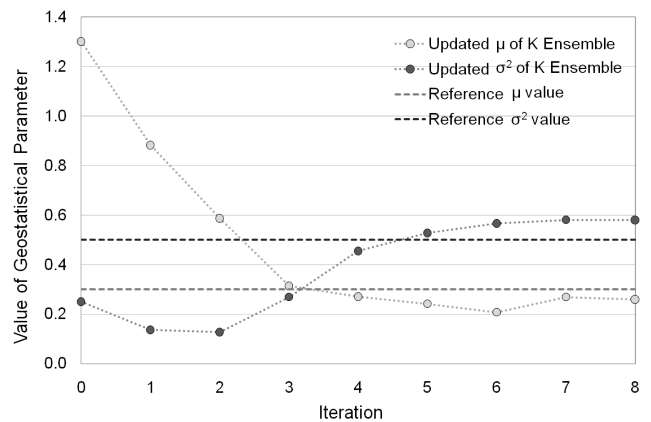

Fig. 14. Progression of the estimated GM parameters and , demonstrating the convergence of the parameter values to ~0.300 log m day^{-1} and 0.580 (log m day^{-1})^2, respectively.

times, however, is seen in the context of observation data error. Figure 9 shows the increase of AE (i.e., the increase in deviation from the true Y_K field) with increasing values of CV of the WT observation data, for the cases when one, two, and four assimilation times are used. Notice that the increase of AE is lessened when observation data from multiple times are assimilated, with the best results occurring when 4 assimilation times are used. The use of additional assimilation times yielded no improvement. For the case of CV = 0.50, the AE value using one, two, and four assimilation times is 0.594, 0.563, and 0.471, respectively.

The second set of update scenarios consists of assimilating observed values of Q from the reference system. The ensemble of values of Q for a given surface grid cell are found to be close to lognormally-distributed (Clark et al., 2008), with the coefficient of determination $r^2 = 0.702$ and the Kolmogorov-Smirnov statistics $KS = 0.270$ for a lognormal fit. This requires both the Q observation data and Q forecast ensemble to be log-transformed before use in the ES update routine.

When $Y_Q = \log Q$ data from 4 gaging stations along stream channel from the four measurement times are assimilated into the forecast ensembles of Y_Q and Y_K, the resulting AE and AEP values of the updated Y_K ensemble are 0.512 and 0.305, providing reductions of 17.3 % and 21.3 % from the forecast values. The ensemble mean for the updated Y_K ensemble for this scenario is shown in Fig. 10. When compared with the updated Y_K ensemble in Fig. 6a, it is clear that observation data from the 24 wells provide an updated Y_K ensemble that fits more closely with the true Y_K field than using Y_Q data. Still, the Y_K ensemble mean in Fig. 10 captures the principal features of the spatial pattern of the true field. However, when error is assigned to the observed Y_Q data, the ability of the Y_Q data to condition the Y_K ensemble is reduced dramatically. Table 2 shows the values of AE and AEP of the updated Y_K ensemble for scenarios in which the CV of the Y_Q data ranges from 0.00 to 1.00. When CV = 0.1,
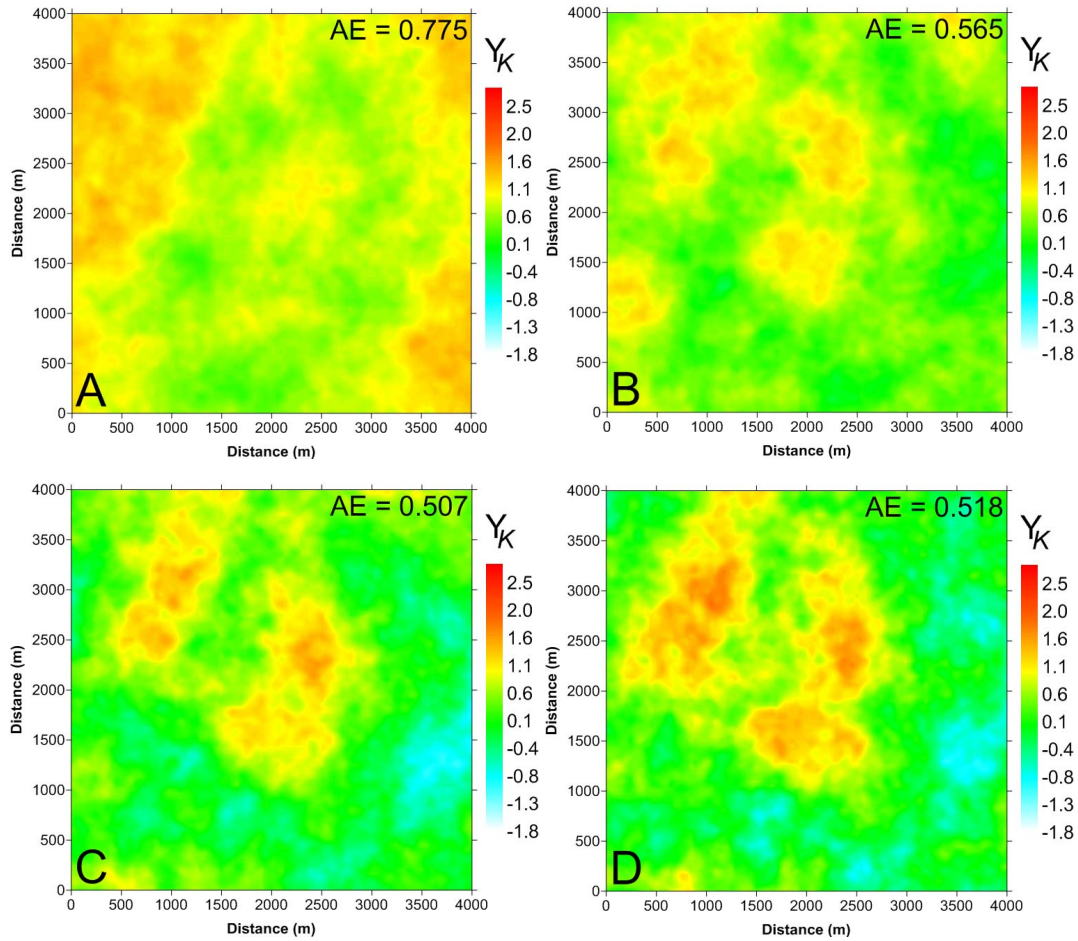
Fig. 15. Ensemble mean of updated Y_K ensemble for the **(A)** 1st iteration, **(B)** 2nd iteration, **(C)** 3rd iteration, and **(D)** 4th iteration, for the case where the true values of and are 0.301 log m day^{-1} and 0.500(log m day^{-1})^2, respectively. Compare to the true state in Fig. 13. The forecast AE values was 1.106.

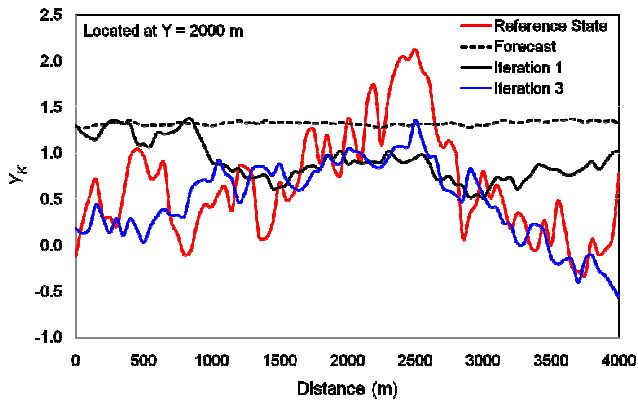**Fig. 16.** Value of Y_K along the $Y = 2000$ m transect for the reference state (red), the foreacast ensemble mean (dotted black line) and the update ensemble mean for the 1st (solid black line) and 2nd (solid blue line) iteration, for the case where the true values of and are 0.301 log m day^{-1} and 0.500 (log m day^{-1})^2, respectively.

the reduction in the AE value from the forecast ensemble is 7.3 %; for CV = 0.30, the reduction is only 2.0 %.

Table 3 presents results of scenarios wherein WT and Y_Q data are jointly assimilated, with the number of observation wells ranging from 2 to 24. In each case, the observation wells are positioned in a grid network. In order to assess the influence of assimilating Y_Q data, four scenarios (1–4) are run with only WT observation data, with the same four scenarios rerun (scenarios 5–8) with the inclusion of assimilating Y_Q data from 4 gaging stations. Results indicate that the inclusion of Y_Q data only provides enhanced conditioning of the Y_K ensemble when the number of observation wells used is less than 8. For example, when 4 observation wells are used, the AE value for the scenarios with and without Y_Q data is 0.455 and 0.434, respectively; when two wells are used, the AE value with and without Y_Q data is 0.545 and 0.482, respectively. Hence, when sparse WT data are available, the additional Y_Q data are able to provide information regarding the spatial distribution of Y_K and hence partially maintain the value of AE.
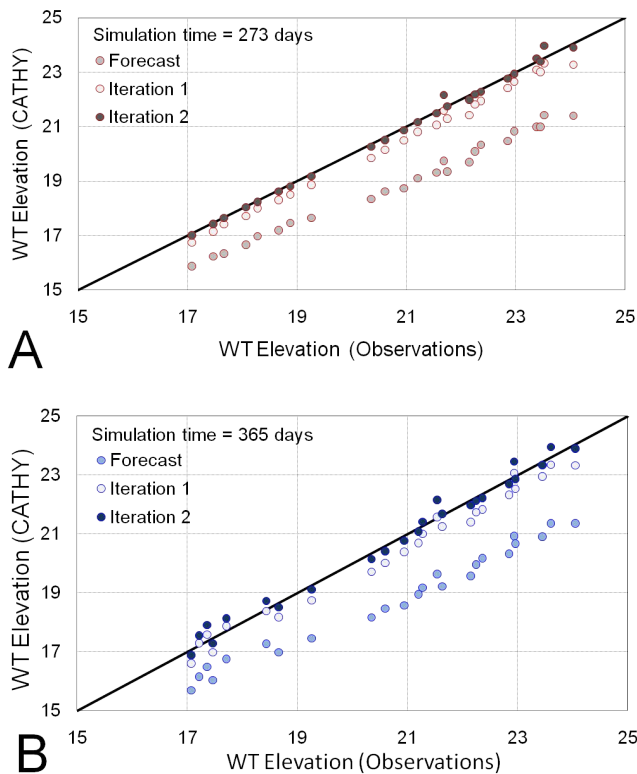
Fig. 17. Comparison between model-calculated WT values and observed WT data from the true system for the forecast WT ensemble, the WT ensemble generated using the updated GM parameter values from the 1st iteration, and the WT ensemble using the updated GM parameters from the 2nd iteration. Comparison are made for (**A**) time = 273 days and (**B**) time = 365 days.

3.3 Case of uncertain geostatistical parameter values

3.3.1 Log-Mean of true Y_K field is uncertain

In this section, the ability of the ES update routine to condition the ensemble of Y_K using WT observation data sampled from a catchment system where μ_{Y_K} is different from the one used in generating the forecast ensemble is explored. In the first scenario, μ_{Y_K} of the true Y_K field is 1.801 log m day^{-1} ($K = 63.2$ m day^{-1}, one-half order of magnitude higher than the forecast value of 20 m day^{-1}); for the second scenario, μ_{Y_K} of the true Y_K field is 0.801 log m day^{-1} ($K = 6.3$ m day^{-1}, one-half order of magnitude lower than the forecast value of 20 m day^{-1}). The value of $\sigma^2_{Y_K}$ in the true systems and the forecast ensemble is the same [(0.250 log m day^{-1})^2]. In Sect. 3.3.2, a more severe test is used to demonstrate the iterative approach described in Sect. 2.5.

The true Y_K field for the first and second scenarios are shown in Fig. 11a and b, respectively. For the two scenarios, the AE of the forecast Y_K ensemble is 0.690 and 0.692, respectively. By assimilating WT data from 24 observation wells for four assimilation times, the AE of the updated Y_K

ensemble for the two scenario is 0.365 and 0.395, respectively, resulting in reductions of 47.1 % and 43.0 % from the forecast AE values. The spatial distribution of the updated Y_K ensemble mean for the two scenarios is shown in Fig. 11c and d. For both scenarios, the updated ensembles capture the general magnitude and spatial distribution of the true Y_K field.

For the first scenario, the initially too-low (compared to the true system) values of Y_K are conditioned to the higher values present in the true system; for the second scenario, the initially too-high values are conditioned to the lower values. The same effect is observed through a comparison between the reference, forecast, and updated values of Y_K across a west-east transect located at Y = 2000 m, as shown in Fig. 12. In both scenarios, the forecast Y_K values along the transect are approximately equal to the forecast μ_{Y_K} value of 1.301, whereas the updated Y_K values have been conditioned to resemble the true profiles.

3.3.2 Iterative approach to discover geostatistical parameter values

To demonstrate the iterative approach, the true aquifer system has μ_{Y_K} and $\sigma^2_{Y_K}$ values of 0.301 log m day^{-1} ($K = 2.0$ m day^{-1}) and 0.500 (log m day^{-1})^2. The resulting true Y_K field is shown in Fig. 13. For each iteration, observation data from 24 observation wells and four assimilations are used to condition the Y_K ensemble. Beginning with a forecast Y_K ensemble generated using $\mu_{Y_K} = 1.301$ log m day^{-1} and $\sigma^2_{Y_K} = 0.250$ (log m day^{-1})^2, eight iterations are performed, with the μ_{Y_K} and $\sigma^2_{Y_K}$ values of the updated Y_K ensemble after each iteration shown in Fig. 14. As seen in Fig. 14, the value of μ_{Y_K} reaches the parameter value from the true system within three iterations, but eight iterations are required to determine if convergence has been achieved. For $\sigma^2_{Y_K}$, the value from the updated Y_K decreases during the first several iterations, but eventually converges upon a value (0.580) slightly higher than the true value of 0.500 (log m day^{-1})^2. If the GM parameter values of the true system were unknown, then it would be assumed that μ_{Y_K} is just under 0.300 log m day^{-1} and $\sigma^2_{Y_K}$ is equal to 0.580 (log m day^{-1})^2.

Besides the convergence to the true GM parameter values, the approach of the updated Y_K ensemble to the spatial distribution of the true Y_K field is demonstrated in Figs. 15 and 16. The ensemble mean of the updated Y_K ensemble for iterations 1 through 4 is shown in Fig. 15a–d, with the AE value generally decreasing from the forecast value of 1.106 (0.755, 0.565, 0.507, and 0.518, respectively), although a slight increase occurs between iterations 3 and 4. The structure of the Y_K spatial distribution, however, progressively approaches the pattern of the true Y_K field shown in Fig. 13 with each successive iteration.

Figure 16 shows the true Y_K values, forecast Y_K values, and the updated values of Y_K for the 1st and 3rd iterations at the Y = 2000 west-east transect. Dramatic improvement

in the updated Y_K values in relation to the true Y_K values occurs from the forecast to the first iteration, and from the first iteration to the third iteration.

Finally, comparisons are made between observed WT data from the true system and model-calculated WT values generated by CATHY using the updated values of μ_{Y_K} and $\sigma^2_{Y_K}$ from the previous iteration. This is especially important since such a comparison, i.e., re-running the numerical model using the estimated parameter values and comparing model results with observed data at observation locations, is generally the only means by which the parameter estimation method can be verified. Figure 17 shows the comparison between observed WT data and model-calculated WT values from the forecast ensemble, the WT ensemble generated using the updated GM parameter values from the first iteration, and the WT ensemble using the updated GM parameters from the second iteration. Comparisons for times = 273 days and 365 days are shown in Fig. 17a and b, respectively.

The match between the forecast values and the true value is much improved upon using the results from the first iteration, and an excellent match occurs using the results from the second iteration. Quantitatively, the sum of squared differences between the model results and true system values is 95.32, 4.29, and 0.59, respectively for time = 273 days, and 99.16, 4.98, and 1.83, respectively for time = 365 days. Notice that the forecasted WT values are lower than the observed WT values from the true aquifer system, since the forecast Y_K values are generated using a higher value of μ_{Y_K}. However, using the lower updated value of μ_{Y_K} from the first and second iterations, the WT values become higher and more in accordance with the observed WT values.

4   Conclusions

The ES update routine, a derivative of the Kalman Filter approach, has been evaluated for the estimation of spatially-variable K in a catchment system using the fully-coupled, surface-subsurface flow model CATHY. A 4.05 km by 4.05 km tilted v-catchment was used in demonstration, with spatio-temporal variability in forcing terms to provide increased uncertainty in the system and to strive to mimic real-world conditions.

Both WT data and Q data were collected from a reference catchment system and assimilated into the ensemble of model results to condition the spatial distribution of K to approach the reference K field. Assimilating WT from a network of observation wells provided a distinct improvement in the K ensemble in relation to the true K field, with sets of data from multiple collection times tempering the decrease in improvement when error was assigned to the observed WT data. Assimilating Q data only slightly improved the K ensemble in relation to the true K field. Jointly assimilating Q and WT data only improved the estimate of K when data from a small number (2,4) of observation wells were

assimilated. This is due to the region of influence of Q, i.e., the regions of the aquifer where the K values directly influence Q and hence can be conditioned by observed values of Q, being small compared to the collective region of influence of WT values at the observation wells.

For cases in which the parameter values defining the geostatistical structure of the aquifer system are uncertain to a small degree (i.e., mean of true K field is one-half order of magnitude different than the assumed mean), the methodology is still able to condition adequately the forecast K ensemble to approach the magnitude and spatial structure of the true aquifer system. For more severe cases, i.e., the true and assumed means are different by an order of magnitude and the true and assumed variance of the K field is different, an iterative process using the ES is used to converge upon the true geostatistical parameter values. Results indicate that the process is successful in approximating the true values.

For the present study uncertainty in the correlation length of the K field is not investigated, and an amendment to the iterative scheme to converge upon unknown correlation length is left to future research, with assimilation of measurements of K likely necessary. Future studies also include an application of the methodology to an actual catchment system in order to estimate the geostatistical parameter values as well as the spatial distribution of K.

Edited by: H. Cloke

References

Ahmed, S. and de Marsily, G.: Cokriged Estimation of Aquifer Transmissivity as an Indirect Solution of the Inverse Problem: A Practial Approach, Water Resour. Res., 29, 521–530, 1993.

Aubert, D., Loumagne, C., and Oudin, L.: Sequential assimilation of soil moisture and streamflow data in a conceptual rainfall-runoff model. J. Hydrol., 280, 145–161, 2003.

Bailey, R. T. and Baù, D. A.: Ensemble Smoother assimilation of hydraulic head and return flow data to estimate hydraulic conductivity, Water Resour. Res., 46, W12543, doi:10.1029/2010WR009147, 2010.

Bailey, R. T. and Baù, D. A.: Estimating spatially-variable first-order rate constants in groundwater reactive transport systems, J. Cont. Hydrol., 122, 104–121, 2011.

Baú, D. A. and Mayer, A. S.: Optimal design of pump-and-treat systems under uncertain hydraulic conductivity and plume distribution, J. Cont. Hydrol., 100, 30–46, 2008.

Bennett, A. F.: Inverse Methods in Physical Oceanography, Cambridge Univ. Press, New York, 1992.

Bixio, A. C., Orlandini, S., Paniconi, C., and Putti, M.: Physically-based distributed model for coupled surface runoff and subsurface flow simulation at the catchment scale, in: Computational

Methods in Water Resources, vol. 2, Computational Methods, Surface Water systems and Hydrology, edited by: Bentley, L. R., Sykes, J. F., Brebbia, C. A., Gray, W. G., and Pinder, G. F., 1115–1122, Balkema, Rotterdam, The Netherlands, 2000.

Boulet, G., Kerr, Y., and Chehbouni, A.: Deriving catchment-scale water and energy balance parameters using data assimilation based on extended Kalman filtering, Hydrol. Sci., 47, 449–467, 2002.

Camporese, M., Paniconi, C., Putti, M., and Salandin, P. :Ensemble Kalman filter data assimilation for a process-based catchment scale model of surface and subsurface flow, Water Resour. Res., 45, W10421, doi:10.1029/2008WR007031, 2009.

Camporese, M., Paniconi, C., Putti, M., and Orlandini, S.: Surface-subsurface flow modeling with path-based runoff routing, boundary condition-based coupling, and assimilation of multisource observation data, Water Resour. Res., 46, W02512, doi:10.1029/2008WR007536, 2010.

Carrera, J. and Neuman, S. P.: Estimation of aquifer parameters under transient and steady-state conditions: 1. Maximum likelihood method incorporating prior information, Water Resour. Res., 22, 199–210, 1986.

Carrera, J., Alcolea, A., Medina, A., Hidalgo, J., and Slooten, L. J.: Inverse problem in hydrogeology, Hydrogeol. J., 13, 206–222, 2005.

Chen, Y. and Zhang, D.: Data assimilation for transient flow in geologic formations via Ensemble Kalman Filter, Adv. Water Resour., 29, 1107–1122, 2006.

Clark, M. P., Rupp, D. E., Woods, R. A., Zheng, X., Ibbitt, R. P., Slater, A. G., Schmidt, J., and Uddstrom, M. J.: Hydrological data assimilation with the ensemble Kalman filter: Use of streamflow observations to update states in a distributed hydrological model, Adv. Water Resour., 31, 1309–1324, 2008.

Drécourt, J.-P., Madsen, H., and Rosbjerg, D.: Calibration framework for a Kalman filter applied to a groundwater model. Adv. Water Resour., 29, 719–734, 2006.

Dunne, S. and Entekhabi, D.: An ensemble-based reanalysis approach to land data assimilation, Water Resour. Res., 41, W02013, doi:10.1029/2004WR003449, 2005.

Durand, M., Molotch, N. P., and Margulis, S. A.: A Bayesian approach to snow water equivalent reconstruction, J. Geophys. Res., 113, D20117, doi:10.1029/2008JD009894, 2008.

Evensen, G.: Using the extended Kalman filter with a multilayer quasi-geostrophic ocean model, J. Geophys. Res., 97, 17905–17924, 1992.

Evensen, G.: Sequential data assimilation with a nonlinear quasi-geostrophic model using Monte Carlo methods to forecast error statistics, J. Geophys. Res., 99, 10143–10162, 1994.

Evensen, G.: The ensemble Kalman filter: theoretical formulation and practical implementation, Ocean Dynam., 53, 343–367, 2003.

Evensen, G.: Data assimilation. The Ensemble Kalman Filter, Springer-Verlag Berlin Heidelberg, 2007.

Evensen, G. and van Leeuwen, P. J., An ensemble Kalman smoother for nonlinear dynamics, Mon. Weather Rev., 128, 1852–1867, 2000.

Fu, J. and Gómez-Hernández, J. J.: Uncertainty assessment and data worth in groundwater flow and mass transport modeling using a blocking Markov chain Monte Carlo method, J. Hydrol., 364, 328–341, 2009.

Gailey, R. M., Crowe, A. S., and Gorelick, S. M.: Coupled process parameter estimation and prediction uncertainty using hydraulic head and concentration data, Adv. Water Resour., 14, 301–314, 1991.

Gautier, Y. and Nœtinger, B.: Geostatistical parameters estimation using well test data, Oil Gas Sci. Technol., 59, 167–183, 2004.

Gómez-Hernández, J. J., Hendricks Franssen, H.-J., and Sahuquillo, A.: Stochastic conditional inverse modeling of subsurface mass transport: A brief review and the self-calibrating method, Stoch. Environ. Res. Risk A., 17, 319–328, 2003.

Hantush, M. M. and Mariño, M. A.: Estimation of spatially variable aquifer hydraulic properties using Kalman filtering, J. Hydraul. Engrg. ASCE, 123, 1027–1035, 1997.

Hendricks Franssen, H. J. and Kinzelbach, W.: Real-time groundwater flow modeling with the Ensemble Kalman Filter: Joint estimation of states and parameters and the filter inbreeding problem, Water Resour. Res., 44, W09408, doi:10.1029/2007WR006505, 2008.

Hendricks Franssen, H. J. and Kinzelbach, W.: Ensemble Kalman filtering versus sequential self-calibration for inverse modeling of dynamic groundwater flow systems, J. Hydrol., 365, 261–274, 2009.

Hendricks Franssen, H. J., Gómez-Hernández, J. J., Capilla, J. E., and Sahuquillo, A.: Joint simulation of transmissivity and storativity fields conditional to steady-state and transient hydraulic head data, Adv. Water Resour., 23, 1–13, 1999.

Hendricks Franssen, H. J., Gómez-Hernández, J. J., and Sahuquillo, A.: Coupled inverse modeling of groundwater flow and mass transport and the worth of concentration data, J. Hydrol., 281, 281–295, 2003.

Hoeksema, R. J. and Kitanidis, P. K.: An application of the geostatistical approach to the inverse problem in two-dimensional groundwater modeling, Water Resour. Res., 20, 1003–1020, 1984.

Hoeksema, R. J. and Kitanidis, P. K.: Analysis of the spatial structure of properties of selected aquifers, Water Resour. Res., 21, 563–572, 1985.

Jafarpour, B. and Tarrahi, M.: Assessing the performance of the ensemble Kalman filter for subsurface flow data integration under variogram uncertainty, Water Resour. Res., 47, W05537, doi:10.1029/2010WR009090, 2011.

Kalman, R. E.: A new approach to linear filtering and prediction problems, J. Basic Eng., 82, 35–45, 1960.

Keppenne, C.: Data assimilation into a primitive-equation model with a parallel ensemble Kalman filter, Mon. Weather Rev., 128, 1971–1981, 2000.

Kitanidis, P. K.: On the geostatistical approach to the inverse problem, Adv. Water Resour., 19, 333–342, 1996.

Kitanidis, P. K. and Vomvoris, E. G.: A geostatistical approach to the inverse problem in groundwater modeling (steady state) and one-dimensional simulations, Water Resour. Res., 19, 677–690, 1983.

Li, B. and Yeh, T.-C. J.: Cokriging estimation of the conductivity field under variably saturated flow conditions, Water Resour. Res., 35, 3663–3674, 1999.

Liu, G., Chen, Y., and Zhang, D.: Investigation of flow and transport processes at the MADE site using ensemble Kalman filter, Adv. Water Resour., 31, 975–986, 2008.

Ngodock, H. E., Jacobs, G. A., and Chen, M.: The representer

method, the ensemble Kalman filter and the ensemble Kalman smoother: A comparison study using a nonlinear reduced gravity ocean model, Ocean Modell., 12, 378–400, 2006.

Orlandini, S. and Rosso, R.: Diffusion wave modeling of distributed catchment dynamics, J. Hydraul. Eng. ASCE, 1, 103–113, 1996.

Putti, M. and Paniconi, C.: Time step and stability control for a coupled model of surface and subsurface flow, in Proceedings of the XV International Conference on Computational Methods in Water Resources (CMWR XV), vol. 2, 1391–1402, Elsevier, New York, 2004.

RamaRao, B. S., LaVenue, A. M., de Marsily, G., and Marietta, M. G.: Pilot point methodology for automated calibration of an ensemble of conditionally simulated transmissivity field 1. Theory and computational experiments, Water Resour. Res., 31, 475–493, 1995.

Reichle, R. H., McLaughlin, D. B., and Entekhabi, D.: Hydrologic data assimilation with the ensemble Kalman filter, Mon. Weather Rev., 130, 103–114, 2002.

Schreider, S. Y., Young, P. C., and Jakeman, A. J.: An application of the Kalman filtering technique for streamflow forecasting in the Upper Murray Basin, Math. Computer Model., 33, 733–743, 2001.

Valstar, J. R., McLaughlin, D. B., te Stroet, C. B. M., and van Geer, F. C.: A representer-based inverse method for groundwater flow and transport application, Water Resour. Res., 40, W05116, doi:10.1029/2003WR002922, 2004.

van Genuchten, M. T. and Nielsen, D. R.: On describing and predicting the hydraulic properties of unsaturated soils, Ann. Geophy., 3, 615–628, 1985.

van Leeuwen, P. J. and Evensen, G.: Data assimilation and inverse methods in terms of probabilistic formulation, Mon. Weather Rev., 124, 2898–2913, 1996.

Wen, W.-H., Deutsch, C. V., and Cullick, A. S.: Construction of geostatistical aquifer models integrating dynamic flow and tracer data using inverse technique, J. Hydrol., 255, 151–168, 2002.

Woodbury, A. D. and Smith, L.: Simultaneous inversion of hydrogeologic and thermal data 2. Incorporation of thermal data, Water Resour. Res., 24, 356–372, 1988.

Xie, X. and Zhang, D.: Data assimilation for distributed hydrological catchment modeling via ensemble Kalman filter, Adv. Water Resour., 33, 678–690, 2010.

Yeh, T.-C. J. and Zhang, J.: A geostatistical inverse method for variably saturated flow in the vadose zone, Water Resour. Res., 32, 2757–2766, 1996.

Yortsos, Y. C. and Al-Afaleg, N.: The permeability variogram from pressure transients of multiple wells: Theory and 1-D application, Soc. Petrol. Eng. J., 2, 328–337, 1997

Zhang, J. and Yeh, T.-C. J.: An iterative geostatistical inverse method for steady flow in the vadose zone, Water Resour. Res., 33, 63–71, 1997.